Regular Article

Dynamics of interacting oxygen ions in yttria stabilized zirconia: bulk material and nanometer thin films

K.L. Ngai[1], J. Santamaria[2], and Carlos Leon[2,a]

[1] Dipartimento di Fisica, Università di Pisa, Largo Bruno Pontecorvo 3, 56127 Pisa, Italy
[2] Grupo de Física de Materiales Complejos, Universidad Complutense de Madrid, 28040 Madrid, Spain

Abstract. The oxygen vacancy dynamics in bulk yttria-stabilized zirconia studied experimentally by conductivity relaxation and quasielastic light scattering had shown anomalous properties that had been attributed to the many-ion effects originating from ion-ion interaction. In the explanation of the anomalous properties given more than ten years ago, some predictions including the actual value of the energy barrier opposing oxygen ion hop have been made but remain unverified. Since then, many molecular dynamics simulations on oxygen vacancy dynamics in bulk YSZ have been published. Moreover, oxygen vacancy dynamics in nanometer thin films of YSZ fabricated in various fashion have been measured by conductivity relaxation as well as studied by computer simulations. This rich collection of new experimental and computer simulations results provide fertile ground for testing the predictions made before. The tests are made and the results are positive. The advance lends considerable support of the previously published explanation of oxygen vacancy dynamics in bulk YSZ. We pointed out that ion dynamics similar to YSZ are found in other ionic conductors, and the explanation for YSZ given here also works there.

1 Introduction

Stabilized zirconia is produced by doping zirconia (ZrO_2) with various aliovalent oxides such as Y_2O_3 and CaO [1–3]. In order to neutralize the excess charge introduced by the dopant cations, Y and Ca, oxygen vacancies are created, giving rise to oxygen ion conductivity. A widely studied stabilized zirconia is yttria-stabilized zirconia (YSZ). This is because of its high oxygen ion conductivity at high temperatures, which makes YSZ attractive in technological applications including oxygen sensors, solid oxide fuel cell (SOFC) electrolytes, etc. With the purpose of gaining an in-depth understanding of oxygen mobility in *bulk* YSZ, many studies have been made by experiments [4–16], and by molecular dynamics simulations [16–24]. A wealth of properties of the dynamics of oxygen ions in bulk YSZ have been revealed by experiments using different techniques, and by various methods of computer simulations. The rich results provide the rare opportunity of gaining a fundamental understanding of ion dynamics in bulk solid state ionic conductors with high concentration of carriers. Actually such an initial attempt has been made in 1998 by using the coupling model (CM) to interpret oxygen ion dynamics in bulk YSZ found by conductivity relaxation and light scattering measurements available before that time [25], and it remains as the only theoretical work that has explained the experimental

data available at that time. Since then, more results on the dynamics of oxygen ion in bulk YSZ have been provided by computer simulations [16–24]. So far no one has compared the rich computer simulation results with the CM interpretations. These relatively new computer simulation results offer excellent opportunities to test consistency with the theoretical explanation given by the CM in the 1998 paper, as will be carried out in this paper.

Furthermore, new developments in the study of oxygen ion dynamics in YSZ are from measurements of the oxygen ion conductivity in thin films with thickness in the nanometer scale. In one study, highly textured thin films of YSZ were deposited onto a MgO substrate [26]. When the film thickness is less than 60 nm, the conductivity is enhanced significantly compared to bulk YSZ. The enhancement increases with decreasing film thickness studied down to 15 nm, and is accompanied by decrease in the activation energy. The observed enhancement is attributed to much high conductivity of the interface layer with estimated thickness of about 1.6 nm, and the increase of measured conductivity is due to increased contribution from interface conductivity with decrease in the film thickness. More recently, yttria-stabilized zirconia (YSZ)/strontium titanate epitaxial heterostructures were fabricated with YSZ film thickness of 62, 30, 20, 5, and 1 nm [27–29]. The lateral oxygen ion conductivity measured in the heterostructures with thin films is very high, up to eight orders of magnitude higher than the bulk near room temperature. From the fact that the enhancement of

[a] e-mail: `carlos.leon@fis.ucm.es`

the conductivity was observed together with the YSZ layer thickness-independent conductance, the high conductivity originates in the interface region. The significant change in dynamics of the oxygen ions when film thickness is reduced to nanometer scale poses a new challenge for explanation.

The paper is organized as follows. In Section 2.1, we give a brief review of the CM and its application to ion dynamics in ionic conductors in general and also in bulk YSZ found by experiments prior to 1998 when the CM was first applied to explain the experimental data [25]. Some predictions on the oxygen ion dynamics in bulk YSZ from the CM have not been tested so far. The collection of results from computer simulations published in the period 2003–2011 [16–24] are introduced in Section 2.2, and are then utilized to test these predictions of the CM. The results of several studies of oxygen ion dynamics in thin films of YSZ with thickness in the nanometer scale by experiments and simulations are introduced in Section 3. The results of nanometer thin films are brought to confront the predictions of the CM in Section 3. A summary is given in Section 4 together with the conclusions.

2 Oxygen ion dynamics in bulk YSZ

2.1 Experimental data and theoretical explanation

The CM [25,30–39] had been applied before to a number of problems on the dynamics, diffusion and conductivity of ions in ionic conductors. The emphasis is put on ion-ion interaction and the pronounced effects it has on the dynamics, as well as the steady state transport coefficients including conductivity and diffusion constant. In the absence of ion-ion interaction, ions move independently, and the ion hopping correlation function, $C(t)$, is an exponential function of time,

$$C(t) = \exp{-(t/\tau_0(T))}, \qquad (1)$$

for all times, where $\tau_0(T)$ is the independent ion hopping relaxation time. In YSZ, $\tau_0(T)$ has the Arrhenius temperature dependence,

$$\tau_0(T) = \tau_\infty \exp(E_a/kT) \qquad (2)$$

where $(\tau_\infty)^{-1}$ is the attempt frequency of oxygen ion to hop over its actual energy barrier E_a. However, the presence of ion-ion interaction introduces correlation between motions of the ions, changing independent motion to co-operative many-ions motions. The interaction potential between ions is anharmonic. For example, the potential used in computer simulations of oxygen ion dynamics in YSZ consists of a Coulomb repulsion the ions and a Born-Meyer-Buckingham potential to account for the short-ranged interactions between the ions [22,24,25]. It is well known from nonlinear Hamiltonian dynamics that the anharmonic interaction potential causes chaos in the phase space [40,41]. According to the CM [42–45], classical chaos changes independent ion relaxation to many-ion

conductivity relaxation with correlation function having the Kohlrausch stretched exponential form,

$$C(t) = \exp[-(t/\tau^*(T))^{1-n}], \quad 0 \leqslant n < 1, \qquad (3)$$

where $\tau^*(T)$ is the conductivity relaxation time. A measure of the effects due to ion-ion interaction is given by n appearing in the exponent in (3), which is appropriately called the coupling parameter. However, chaos only starts after a characteristic time, t_c, the magnitude of which is determined by the interaction potential [46]. Consequently, (2) holds only for $t > t_c$, and (1) is still valid for $t < t_c$. The crossover of the correlation function from (1) to (3) in a neighborhood centered at $t = t_c$ has been observed by high frequency measurement on glassy and crystalline ionic conductors from which the value of $t_c \approx 1$ to 2 ps has been determined. References are given in a recent review by León et al. [39]. Moreover, the crossover at t_c gives rise to the relation,

$$\tau^*(T) = \left[t_c^{-n}\tau_0(T)\right]^{1/(1-n)}, \qquad (4)$$

which has been used to explain quantitatively many experimental facts of ion dynamics including the isotope mass dependence of the conductivity [47], and the difference between NMR and conductivity relaxations [31]. In several ionic liquids, the independent ion hopping relaxation was observed together with the many-ion conductivity relaxation in the isothermal electric loss modulus spectra [48–50], and the two relaxation times $\tau^*(T)$ and $\tau_0(T)$ are related by (4) for different combinations of temperature and pressure. Hence, the reality of the independent relaxation time $\tau_0(T)$ is supported by experiments.

The combination of equations (2) and (3) leads to the following expressions for the $\tau^*(T)$:

$$\tau^*(T) \equiv \tau^*_\infty \exp(E_a^*/kT) \qquad (5)$$

where

$$\tau^*_\infty = [t_c^{-n}\tau_\infty]^{1/(1-n)} \qquad (6)$$

and

$$E_a^* = E_a/(1-n). \qquad (7)$$

Thus, ion-ion interaction makes the experimentally observed prefactor τ^*_∞ and the apparent activation energy E_a^* different from τ_∞ and E_a respectively. The predictions of the CM given by equations (1)−(7) have been applied to and successfully verified by experiments in various glassy and crystalline ionic conductors. Some examples given in a recent review [39] include the glassy 0.5AgI–0.5AgPO$_3$ and 0.5Ag$_2$S–0.5GeS$_2$, the crystalline lithium fast-ion conductor Li$_{0.18}$La$_{0.61}$TiO$_3$ (LLTO), and the oxygen ion dynamics in the pyrochlores, Gd$_2$Ti$_{2-y}$Zr$_y$O$_7$, with $0.5 \leqslant y \leqslant 2$. In the case of the pyrochlores, Gd$_2$Ti$_{2-y}$Zr$_y$O$_7$, the experiment by Moreno et al. [51] had determined the Arrhenius activation energy E_a^* and n for different composition, y. The conductivity originates from oxygen ions jumping from $48f$ sites to $48f$ sites. The energy barrier for this jump obtained by molecular dynamics simulations is $0.57−0.64$ eV [52–54] and by static lattice energy minimization simulations is 0.58 eV [55]. On the other hand,

the experimental E_a^* is significantly larger. Using (7), the actual energy barrier of oxygen ions to jump from E_a, can be calculated by the product, $(1-n)E_a^*$. The value $E_a = 0.60$ eV was obtained, in good agreement with simulations.

Application of the CM to oxygen ion dynamics in YSZ starts from the determination of the coupling parameter n and $\tau^*(T)$, as well as τ_∞^* and E_a^*, from the conductivity relaxation data obtained at low frequencies ω satisfying the condition $\omega t_c \ll 1$. The procedure is to fit the isothermal conductivity relaxation data expressed in terms of the complex electric modulus $M^*(\omega)$ by the Fourier transform of the stretched exponential form of $C(t)$ in (3) [56], i.e.,

$$M^*(\omega) = M' + iM''$$

$$= M_\infty \left[1 - \int_0^\infty dt \exp(-i\omega t)(-dC(t)/dt) \right]. \quad (8)$$

Here, M_∞ is the reciprocal of ε_∞, the high frequency dielectric constant. The complex conductivity is related to $M^*(\omega)$ by the Maxwell relation, $\sigma^*(\omega) = i\omega\varepsilon_0\varepsilon^*(\omega) = i\omega\varepsilon_0/M^*(\omega)$. The d.c. conductivity, σ_{dc}, is related to $\tau^*(T)$ by the expression [56],

$$\sigma_{dc} = \varepsilon_0\varepsilon_\infty/\langle\tau^*(T)\rangle \quad (9)$$

where $\varepsilon_o = 8.854 \times 10^{-14}$ F/cm is the permittivity of free space. In equation (9), $\langle\tau^*(T)\rangle$ is the average conductivity relaxation time obtained by integration over time of $C(t)$ in (3), and is related to $\tau^*(T)$ by

$$\langle\tau^*(T)\rangle = [\Gamma(1/\beta)/\beta]\tau^*(T), \quad (10)$$

where $\beta = (1-n)$, and Γ is the gamma function. The d.c. conductivity, σ_{dc}, of YSZ had been measured over a broad temperature range. Figure 1 shows some representative sets of data at high temperatures [5–7,10] and one set of data of bulk YSZ with 9.5 mol% Y_2O_3 at lower temperatures by León et al. [12]. The latter have Arrhenius dependence and the activation energy is 1.16 eV as illustrated in Figure 1. At higher temperatures, the Arrhenius temperature dependence of σ_{dc} no longer holds with the apparent activation energy decreasing monotonically with increasing temperature to reach the value of about 0.49 eV as indicated by the dashed line in Figure 1.

The procedure to analyze conductivity relaxation data outlined in the above was carried out by León et al. [12]. By fitting their electric modulus data of bulk YSZ with 9.5 mol% Y_2O_3, they found $n_b = 0.57$ which is temperature independent. The temperature dependence of τ^* is Arrhenius, with the activation energy of 1.16 eV, same as that of σ_{dc} shown before in Figure 1, consistent with the relation between these two quantities given by equations (9) and (10). The data of $\tau^*(T)$ are shown by brown closed squares in Figure 2. The pale blue straight line through the data points of the YSZ with 9.5 mol% Y_2O_3 has activation energy $E_a^* = 1.16$ eV, and given by the expression,

$$\tau^*(T) \equiv \tau_\infty^* \exp(E_a^*/kT) = 10^{-16.44} \exp(1.16 \text{ eV}/kT) \text{ s.} \quad (11)$$
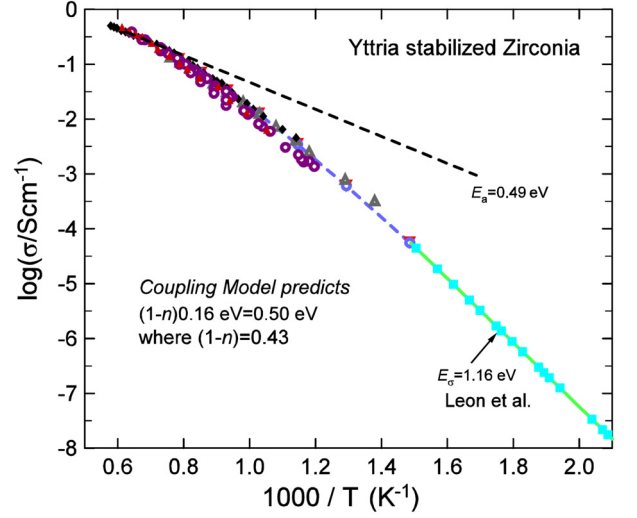

Fig. 1. (Color online) Temperature dependence of d.c. conductivity data of bulk YSZ. Pale blue squares strung together by green line are lower temperature data from León et al. [12] of bulk YSZ with 9.5 mol% Y_2O_3. Higher temperature data: black closed diamonds from Casselton [5]; purple open circle from Dixon et al. [6]; red closed triangles from Stricker and Carlson [10], and grey open triangles from Näfe [7]. The dashed line indicates the high temperature activation energy of approximately 0.49 eV.

The independent hopping relaxation times, $\tau_0(T)$, calculated from τ^* via (6) with $t_c = 2$ ps, is

$$\tau_0(T) \equiv \tau_\infty \exp(E_a/kT) = 10^{-13.74} \exp(0.50 \text{ eV}/kT) \text{ s.} \quad (12)$$

It is remarkable that the activation energy $E_a = 0.50$ eV deduced from $E_a^* = 1.16$ eV from data at low temperatures by the CM equation (7) almost coincides with the asymptotic high temperature activation energy of σ_{dc} determined to have the value of 0.49 eV in Figure 1. This coincidence is not an accident. According to equations (9) and (10), $\tau^*(T)$ is near the crossover time $t_c = 2$ ps at high temperatures where σ_{dc} reaches the large value of 1 S/cm in Figure 1. Thus σ_{dc} measured at the high temperature regime in Figure 1 is governed by the independent hopping relaxation times, $\tau_0(T)$, and hence have the activation energy $E_a = 0.50$ eV as deduced from lower temperature conductivity relaxation data via the CM equation (7).

The results of $\tau^*(T)$ and $\tau_0(T)$ from the conductivity relaxation data of León et al. and given by equations (11) and (12) are represented by the pale blue solid and green dashed lines, respectively, in Figure 2. The corresponding $\tau_0(T)$, calculated with $t_c = 1$ ps is shown by the purple dotted line near the green dashed lines. The only difference for the choice of $t_c = 1$ ps is the prefactor τ_∞ has the value of $10^{-13.91}$. All three lines are extended to temperatures higher and lower than the range of conductivity relaxation data of León et al. shown by brown closed squares in Figure 2. Included in Figure 2 are the lower temperature data of $\tau^*(T)$ deduced from the conductivity relaxation measurement by Rivera et al. [14] of a single crystal and a 700 nm thick thin film of YSZ with 8 mol%
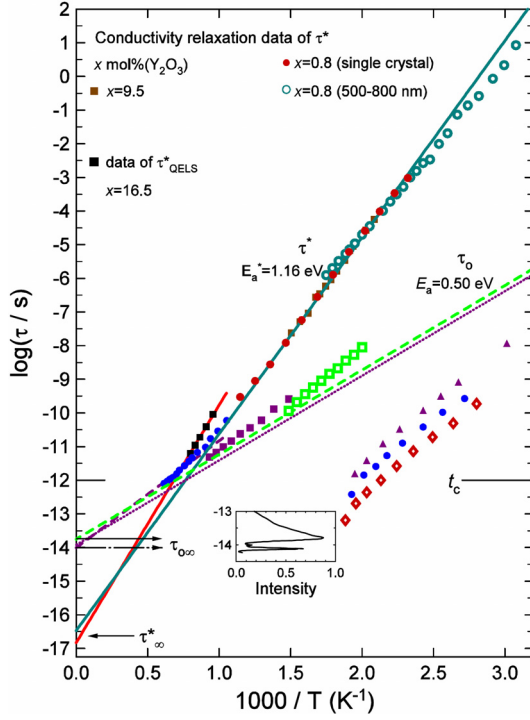
Fig. 2. (Color online) Arrhenius plots of various relaxation times of oxygen ions in bulk YSZ and thin films of YSZ. The conductivity relaxation times $\tau^*(T)$ and quasielastic light scattering correlation time $\tau^*_{QELS}(T)$ were obtained in bulk YSZ samples with mol% of Y_2O_3 and symbols used to represent them indicated. The pale blue and red solid lines are Arrhenius fits to the data of τ^* and τ^*_{QELS}, respectively. The blue closed circles within the range, $0.6 < 1000/T < 1.1$ are $\tau^*(T)$ calculated from one set of high temperature d.c. conductivity data in Figure 1. The green broken line and the purple dotted line are the independent ion hopping relaxation time $\tau_0(T)$ calculated from $\tau^*(T)$ by equation (4) with $t_c = 2$ and 1 ps, respectively. The intercepts of the Arrhenius fits to $\tau^*(T)$ and τ^*_{QELS} with the y-axis at infinite temperature give the prefactors, $\tau^*_\infty = 10^{16.44}$ s and $\tau^*_{QELS,\infty} = 10^{-16.82}$ s, respectively. On the other hand, the intercept of the Arrhenius T-dependence of $\tau_0(T)$ with the y-axis yields the prefactor $\tau_{0\infty}$ in good agreement with the reciprocal of the angular frequency corresponding to the narrow band at 690 cm^{-1} of the hyper-Raman spectra converted to time and shown in the inset. The data of the conductivity relaxation times, $\tau^*_S(T)$, of 15 nm YSZ thin film deposited on MgO are shown by closed purple squares located just above the green dashed line representing $\tau_0(T)$. The $\tau^*_S(T)$ of 62, 30, 5, and 1 nm YSZ thin film sandwiched between two 10 nm STO layers are shown by green open squares (near and above the green dashed line), closed purple triangles, closed blue circles, and open red diamonds (below the green dashed line), respectively.

of Y_2O_3. The difference in $\tau^*(T)$ between León et al. and Rivera et al. is not large, although $n_b = 0.55$ reported by Rivera et al. is slightly smaller, and $E_a = 0.52$ eV is slightly larger. Also included in Figure 2 are $\tau^*(T)$ calculated by equations (9) and (10) from one set of high temperature data in Figure 1. These are shown by blue

closed circles located within the region in Figure 2 where the lines representing $\tau^*(T)$ and $\tau_0(T)$ intersect.

The prefactor, τ^*_∞, of the experimentally observed conductivity relaxation time τ^* is very short and its reciprocal corresponds to an unphysically high attempt frequency, ω^*_∞, of the oxygen ions. High attempt frequencies of a similar magnitude (e.g., $\omega^*_\infty = 10^{-15.8}$ s^{-1} for YSZ with 10 mol% Y_2O_3) have been previously reported [13], further corroborating this finding. On the other hand, the reciprocal of the prefactor τ_∞ of $\tau_0(T)$ has the magnitude of an attempt frequency. The actual attempt frequency of oxygen ions in YSZ was determined experimentally from the hyper-Raman spectrum obtained by Shin and Ishigame [8]. The hyper-Raman spectrum (intensity versus frequency shift plot) of a YSZ sample of $(ZrO_2)_{1-x}(YO_{1.5})_x$ with $x = 0.18$, corresponding to 9 mol% of Y_2O_3, is converted to a plot of intensity versus $\omega^{-1} \equiv (2\pi f)^{-1}$ in units of s^{-1} and shown as the inset in Figure 1. The vibrational modes shown have displacement of the oxygen ion towards the vacancy and are candidates for the attempt frequency of independent ion hop. It was argued by Shin and Ishigame that the highest frequency narrow band located at 690 cm^{-1}, corresponding to time of $10^{-14.1}$ s, contributes most effectively to the hopping of the oxygen ions and can be identified with their attempt frequency. Since the intensity and location of the band at 690 cm^{-1} does not vary much with the mol% of yttria, we can employ the hyper-Raman data of the $(ZrO_2)_{1-x}(YO_{1.5})_x$ with $x = 0.18$ to locate the attempt frequency of the oxygen ions in the sample of León et al. with similar mol% of yttria.

Having determined the reciprocal of the true attempt (angular) frequency ω_{att} of the oxygen ions from experiment to be $10^{-14.1}$ s, comparison of it can be made in Figure 1 with the prefactors τ^*_∞ and τ_∞. The true angular attempt frequency $(\tau_\infty)^{-1}$ deduced from the coupling model is only 2.4 (for $n_b = 0.57$) and 1.6 (for $n_b = 0.55$) times smaller than the experimentally determined ω_{att}. This small discrepancy between $(\tau_\infty)^{-1}$ and ω_{att} is well within the uncertainty in determining τ_0 from (6) due to errors in n_b and τ^* obtained from experiments. On the other hand as mentioned earlier, the angular frequency $(\tau^*_\infty)^{-1} = 10^{16.44}$ s^{-1} is unphysical because its value is too high. In fact it is more than two hundred times larger than the actual attempt frequency ω_{att}. According to the coupling model, the unphysically high value of $(\tau^*_\infty)^{-1}$ is caused by many-ion correlations between the hopping ions. Also the actual energy barrier for oxygen ion hop is $E_a = 0.52$ eV. On the other hand, the observed activation energy of the d.c. conductivity, $E^*_a = 1.16$ eV, is not the actual barrier. Its larger value comes from the correlations and cooperativity intrinsic to the dynamics of interacting ions.

Quasielastic light scattering (QELS) in YSZ by tandem Fabry-Perot interferometry was measured by Suemoto and Ishigame [11] using the same samples as in the hyper-Raman scattering experiment. Light scattering is due to fluctuation of the polarizability caused by ionic motion. They found that the shape of the scattered light

intensity peak as a function of temperature taken at constant frequency, f, in the range from 1.8 to 24 GHz is non-Lorentzian and in good agreement with that coming from a correlation function that has the Kohlrausch form as predicted by the CM. The dependence of the temperature of the intensity maximum on f is converted to a dependence on $(2\pi f)^{-1} \equiv \tau_{QELS}^*$ and the data are shown in Figure 1. The thinner straight line through the data point is the best fit to the Arrhenius temperature dependence

$$\tau_{QELS}^* \equiv \tau_{QELS,\infty}^* \exp(E_{a,QELS}^*/kT)$$
$$= 10^{-16.82} \exp(1.40 \ \text{eV}/kT)\,\text{s} \qquad (13)$$

obtained by Suemoto and Ishigame [11]. The unphysically high apparent attempt frequency $\tau_{QELS\infty}^*$ is again evident from equation (12). The spectral shape is well fitted by an expression proportional to $\chi''(\omega)/\omega$, where $\chi''(\omega)$ is the imaginary part of the susceptibility function calculated [11] by a Fourier transform of the time derivative of the Kohlrausch function, equation (3). In the process, the coupling parameter n_{QELS} was determined to have the value of 0.55. The independent ion hopping correlation time, $\tau_{QELS,0}$, calculated from τ_{QELS}^* via (6) has the Arrhenius dependence,

$$\tau_{QELS,0}(T) \equiv \tau_{QELS,\infty} \exp(E_{a,QELS}/kT)$$
$$= 10^{-14.0} \exp(0.63 \ \text{eV}/kT)\,\text{s} \qquad (14)$$

and is plotted as a function of temperature in Figure 1 (the thinner dashed line).

The situation in QELS is similar to conductivity relaxation in that the experimentally determined attempt frequency, $(\tau_{QELS,\infty}^*)^{-1} = 10^{16.82}$ radians/s, is too high to be real. However, the attempt frequency, $(\tau_{QELS,\infty})^{-1} = 10^{14.0}$ radians/s, of the independent ionic hopping motion deduced by the CM nearly coincides with the measured frequency of the vibrational mode (690 cm^{-1}). Thus, the QELS data reaffirm the interpretation of the CM that τ_{QELS}^* and $\tau_{QELS,0}$ are the ion hopping correlation times with and without the effects of many-body interactions between the ions, respectively. Moreover, $E_{a,QELS} = 0.63$ eV is the actual energy barrier that the oxygen has to overcome, and the larger $E_{a,QELS}^* = 1.4$ eV is due to enhancement by the many-ion dynamics.

There is support that the smaller $E_a = 0.52$ eV and $E_{a,QELS} = 0.63$ eV deduced by the CM via (6) is the actual energy barrier from the d.c. conductivity, σ_{dc}, of YSZ samples with 9.5 to 16.5 mol% of Y_2O_3 measured up to high temperatures by various groups [5,6,10]. As shown before in Figure 1 of the 1998 paper, when σ_{dc} exceeds 0.1 S/cm, its temperature dependence becomes weaker than the Arrhenius dependence with activation energy, E_a^*, established at lower temperatures. On further increase of temperature and as σ_{dc} approaches 1 S/cm, the asymptotic activation energy is about 0.49 eV, nearly the same as $E_a = 0.52$ eV. As σ_{dc} approaches 1 S/cm, the conductivity relaxation time $\langle\tau^*(T)\rangle$ calculated by (9) is near $t_c = 1$ to 2 ps [25]. Hence, the high temperature behavior of σ_{dc} is consistent with CM on the crossover of the

ion hopping correlation function from equation (3) to (1) at $t_c = 1$ to 2 ps, with the corresponding change of activation energy from E_a^* to E_a. The observed asymptotic activation energy of 0.49 eV at high temperatures is an independent estimate of the actual energy barrier, which is in agreement with its value deduced at lower temperatures from E_a^* and the CM (7).

2.2 Computer simulations data compared with theoretical interpretation

Computer simulations of oxygen ion dynamics in YSZ using various methods have been published by many groups. The results generated have fundamental significance and are critical for testing the predictions of the CM. The migration energy barriers and the self-diffusion of oxygen at macroscopic time-scale had been calculated by kinetic Monte Carlo (kMC) simulation with density functional theory [17]. The method assumes that oxygen diffusion is well-represented by oxygen vacancy hopping through the edges of cation tetrahedra. The advantage of this method is that it is not restricted to relatively short times like molecular dynamics simulations. For example, the smallest of all the activation barriers for oxygen vacancy migration is across the Zr–Zr edges, and it is 0.58 eV. Activation energy for oxygen self-diffusion, E_{Ka}, increases with y, the mol % of Y_2O_3, from nearly 0.58 eV for y less than 2.5 to $\approx$0.59 eV for $y = 8$, $\approx$0.60 eV for $y = 10$, and $\approx$0.61 eV for $y = 12$. It was pointed out in reference [22] that these migration energy barriers were calculated without including ionic interactions. This may explain why the calculated migration energy barriers E_{Ka} are smaller than E_a^* and $E_{a,QELS}^*$ found in conductivity and quasielastic light scattering experiments, say for 8 mol% of Y_2O_3. Notwithstanding, these smaller activation energies E_{Ka} calculated without ion-ion interaction is the actual energy barrier, and hence it can be identified with the energy barrier for independent oxygen hop, E_a, of the CM in (2). It is clear that $E_{Ka} \approx 0.59$ eV for $y = 8$ mol% lies close and in between the two values of the energy barrier for independent oxygen hop: $E_a \approx 0.52$ eV and $E_{a,QELS} = 0.63$ eV deduced from conductivity relaxation and quasielastic light scattering, respectively. Thus, the result of $E_{Ka} \approx 0.60$ eV from the simulations in reference [17] supports the prediction of the CM that the true energy barrier E_a of oxygen ion hopping is in the range $0.52 \leqslant E_a \leqslant 0.63$ eV, which has not been tested before.

Recognizing the importance of accounting for ionic interactions, a kinetic Monte Carlo model was used to calculate ionic conductivity in single-crystal YSZ [22]. The kinetic Monte Carlo model [22] was based on combining density functional theory with the cluster expansion method. The results of ionic conductivity of YSZ with 8 mol% of Y_2O_3 showed an increase of the activation energy to 0.74 eV at high T and 0.85 eV at low T, as compared with $E_{Ka} \approx 0.59$ eV. The enhancement of the activation energy found by including ion-ion interaction in the simulations of Lee et al. [22] is in accord with the prediction

of the CM in (7), although the size is still smaller than $E_a^* = 1.16$ eV found by conductivity relaxation data.

Another molecular dynamics simulation in which the interaction between oxygen ions was included was published by Tarancón et al. [24]. The potential energy chosen is a function of the distance between ions, Zr^{4+}, Y^{3+}, and O^{2-}. It is composed of a Born-Mayer-Buckingham potential for short range interactions, and Coulomb terms to describe the long-range electrostatic interactions between the ions of YSZ. These authors obtained the oxygen tracer diffusion coefficient of YSZ with 8 mol% Y_2O_3 at high temperatures ranging from 1159 K to 1959 K. From the Arrhenius temperature dependence, they obtained the activation energy of 0.68 eV, which is significantly smaller than $E_a^* = 1.16$ eV of d.c. conductivity at lower temperatures. Expressed in terms of $1000/T$, the temperature range of the simulations corresponds to $0.51 \leqslant 1000/T \leqslant 0.86$ K^{-1}. As can be seen by inspection of Figure 1, in this temperature range, overall the conductivity relaxation time τ^* has a much weaker T-dependence than its Arrhenius T-dependence established at lower temperatures with $E_a^* = 1.16$ eV. Its apparent activation energy is significantly smaller than 1.16 eV, but still larger than $E_a \approx 0.52$ eV and $E_{a,QELS} = 0.63$ eV. Therefore, the activation energy of 0.68 eV found by Tarancón et al. is due to τ^* not long compared with $t_c \approx 1$ to 2 ps in the temperature range of simulations, consistent with the existence of the crossover from many-ion relaxation to independent ion hop in the CM.

Similar molecular dynamics simulations of YSZ were carried out by Devanathan et al. with the same potential [19] also at high temperatures from 1125 to 2500 K. The diffusion coefficients of oxygen obtained over this range have activation energies of 0.59, 0.60, and 0.73 eV for YSZ with 6, 8, and 10 mol% Y_2O_3, respectively. Again, τ^* is close to $t_c \approx 1$ to 2 ps in the measurement temperature range, and the activation energies obtained by Devanathan et al. are the actual energy barriers opposing oxygen hopping consistent with the values deduced by the CM.

Mean square displacements of oxygen in YSZ were obtained by Chang et al. [57] over the temperature range, $873 \leqslant T \leqslant 1473$ K for times up to 500 ps in another molecular dynamics simulation using the same potential. For the YSZ with 7 mol% Y_2O_3, we obtain the activation energy of about 0.5 eV. For the same reason as discussed in the above, the proximity of τ^* to $t_c \approx 1$ to 2 ps in the simulation temperature range justifies interpreting the deduced activation energy of 0.5 eV as the actual energy barrier of oxygen vacancy hopping.

Another similar molecular dynamics simulation by Lau and Dunlap [23] up to 2.5 ns reported d.c. conductivity of single crystal YSZ with 8 mol% Y_2O_3 having Arrhenius temperature dependence over about 15 orders of magnitude in the wide temperature range from 300 to 1400 K, and have activation energy of 0.59 ± 0.05 eV. This activation energy is similar to $E_a \approx 0.52$ eV and $E_{a,QELS} = 0.63$ eV and is consistent with the interpretation of actual energy barrier as long as temperature is higher than say

1000 K. However, the results of Lau and Dunlap at temperature below say 800 K are at odds with the much larger activation energy, $E_a^* = 1.16$ eV, of d.c. conductivity observed by experiments of single crystal YSZ with 8 mol% Y_2O_3, as shown in Figure 1.

There is a finite-temperature dynamical simulations of the oxygen vacancy dynamics in bulk cubic zirconia by Pennycook et al. [58,59], where the oxygen vacancies were generated by applying 7% strain to change the oxygen sublattice. At high temperatures the oxygen structure becomes disordered. The mean-square-displacements were calculated up to 6 ps, and hence the diffusion coefficients of oxygen in the strained structure were obtained from the simulations. The activation barrier extracted from an Arrhenius plot of the diffusivities is 0.4 ± 0.1 eV, identical to $E_a \approx 0.50$ to 0.52 eV within the error estimate. Since the simulations were carried out only up to 6 ps and close to $t_c \approx 1$ to 2 ps, this activation energy from simulation of strained bulk cubic zirconia can be taken as another source of information on the actual energy barrier for oxygen diffusion. The effect of strain has been also recently examined by using static atomistic simulations, based on empirical pair-potentials (EPP) [60] to determine the energetic barriers for oxygen-vacancy migration in a fluorite-structured lattice without considering ion-ion interactions. Authors of that work find a migration activation enthalpy of 0.59 eV in unstrained material (in good agreement with the estimates using the CM). They further propose that strain may account for large increases (up to 6 orders of magnitude) of the oxygen conductivity and that increased migration entropy (preserving the fluorite structure) may account for an additional order of magnitude conductivity increase.

3 Oxygen ion dynamics in YSZ thin films

A recent trend in the research field of solid state ionics is to study the changes of ionic conductivity if any when dimension of the material is reduced to nanometer length-scale [61,62]. In stabilized zirconia samples containing 1.7 and 2.9 mol% Y_2O_3 with average grain sizes of $25-50$ nm, Mondal et al. [63] reported that the specific grain boundary conductivities of the nanocrystalline samples is $1-2$ orders of magnitude higher than that of the microcrystalline samples. Maier and collaborators [64,65] found two to three orders of magnitude increase of the d.c. ionic conductivity in nano-crystalline CaF compared to coarse-grained CaF, and also in superlattices of CaF_2 and BaF_2 when the thickness of the individual layers was decreased down to 16 nm.

3.1 Thin films of YSZ deposited on MgO substrates

In highly textured thin films of YSZ with 9.5 mol% Y_2O_3 deposited on MgO substrates and thicknesses between 60 and 15 nm, Kosacki et al. [26] found enhanced conductivity. The d.c. conductivity, σ_{dc}, in the 15 nm film is about 2 orders of magnitude higher than 2000 nm thick films at

673 K. Its activation energy is 0.62 eV, which is significantly lower than 1.09 eV of the 2000 nm thick film [26] and 1.16 eV of the bulk samples shown in Figure 2 with the same composition. The d.c. conductivity, σ_{dc}, data of the 15 nm film from Kosacki et al. are converted to $\tau^*(T)$ via (9), and the results are shown by purple closed squares lying just above the dashed green line representing equation (12) for $\tau_0(T)$ in Figure 2. From the dependence of σ_{dc} on film thickness, Kosacki et al. concluded that the bulk conductivity and the surface/interface conductivity contribute in parallel. The surface/interface contribution becomes more important in thinner film. Using a mixture model to separate one contribution from the other, Kosacki et al. deduced that the surface/interface conductivity is about three to four orders of magnitude higher than that of the bulk, and its activation energy is 0.45 eV. These results are interesting but one should be mindful that they are dependent on the mixture model used to analyze the data. How exactly the two contributions have to be put together to become the observed σ_{dc} in the thin films is an open question. Notwithstanding, the results suggest the activation energy of the surface/interface conductivity is 0.62 eV as observed or less. This experimental fact is important for the thrust of the present paper. At surface/interface of YSZ, interaction between oxygen ions is weaker than in the bulk because of the absence of mobile oxygen ions (i.e. absence of oxygen vacancies) across the surface/interface. Weaker ion-ion interaction at the surface/interface leads to coupling parameter, n_S, smaller than $n_b = 0.55-0.57$ for the bulk. It follows from the CM (7), that the activation energy of the surface/interface conductivity, $E_{a,S}^*$, given by

$$E_{a,S}^* = E_a/(1 - n_S), \tag{15}$$

is smaller than the activation energy of the bulk, $E_a^* = 1.15$ eV, because n_S is less than n_b, and the actual energy barrier, E_a, is the same in the bulk or at the surface/interface. This feature, i.e. $E_{a,S}^* < E_a^*$, is consistent with the experimental data, also can be gleaned from Figure 2.

Furthermore, equation (4) for the bulk conductivity relaxation time $\tau_b^*(T)$ can be written as,

$$\tau_b^*(T) = \tau_0(T)[\tau_0(T)/t_c]^{n_b/(1-n_b)}. \tag{16}$$

Apply the same for the surface/interface conductivity relaxation time, $\tau_S^*(T)$, we have

$$\tau_S^*(T) = \tau_0(T)[\tau_0(T)/t_c]^{n_S/(1-n_S)}. \tag{17}$$

Since the exponent, $n/(1 - n)$, is a monotonic increasing function of n, and $(\tau_0/t_c) \gg 1$, it follows from equations (16) and (17) that $\tau_S^*(T)$ is much shorter than $\tau_b^*(T)$ because n_S is less than n_b. Again this feature is in agreement with the experimental data. It is possible at the surface there is an additional entropy contribution that enhanced oxygen hopping rate, and further reduce $\tau_S^*(T)$ than obtained from (17).

3.2 Interfaces of epitaxial ZrO₂:Y₂O₃/SrTiO₃ heterostructures

Thinner the YSZ film, more important is the influence of the surface/interface in reducing the ion-ion interaction, and naturally n_S becomes smaller. The consequences are larger decrease in $E_{a,S}^*$ to approach the actual energy barrier, E_a, and higher d.c. conductivity or shorter $\tau_S^*(T)$. These trends were found by Garcia-Barriocanal and collaborators [28,29] in a trilayer heterostructure where a film of YSZ with 8 mol% Y₂O₃ were sandwiched between two 10-nm-thick layers of insulating SrTiO₃ (STO). The YSZ film thickness ranges from 62 nm down to 1 nm. In addition, superlattices alternating 10-nm thick STO layer with the YSZ film were fabricated. The interfaces between the STO and the YSZ are atomically flat, with the YSZ perfectly coherent with the STO. Due to large mismatch between the lattice constants of STO and YSZ, the epitaxial growth of the YSZ on top of the STO engenders a large expansive strain in the thin YSZ layers of 7% in the ab plane. Garcia-Barriocanal et al. have made conductivity relaxation measurements to determine the d.c. conductivity, which they have ascertained by other measurement that it comes from oxygen ionic diffusion, and (non dispersive) electronic contribution is negligible. In the following discussion it is assumed that the observed conductivity is in fact due to an enhanced ionic conductivity. This interpretation has been questioned by some authors which favor an electronic origin of this large conductivity [66,67]. The transfer of vacancies to the STO may dope it with electrons [60] which could give a dispersive contribution to the conductivity due to the hopping between isolated trap states. Tracer diffusion experiments may help in identifying the nature of the enhanced conductivity [68]. Garcia-Barriocanal's data of σ_{dc} are converted here to $\tau_S^*(T)$ via (9), and the temperature dependence of $\tau_S^*(T)$ for [STO₁₀ ₙₘ/YSZ$_{X\,nm}$/STO₁₀ ₙₘ] trilayers with $X = 62$, 30, 5, and 1 nm thick YSZ films are shown in Figure 2. Represented by open green squares, $\tau_S^*(T)$ of the 62 nm YSZ film show a decrease of about two orders of magnitude than $\tau_b^*(T)$ at the measurement temperature range, and the activation energy of $\tau_S^*(T)$ decreases to 0.72 eV from 1.16 eV for $\tau_b^*(T)$. On decreasing the thickness of the YSZ layer to 30 nm, $\tau_S^*(T)$ decreases another three orders of magnitude, and the activation energy decreases to 0.6 eV. On further decrease of the thickness to 5 nm and all the way down to 1 nm (two unit cells of YSZ), the conductivity increases and the corresponding $\tau_S^*(T)$ decreases inversely as the thickness of the YSZ layer. The d.c. conductivity of the 1-nm YSZ layer shows a exceedingly high value of 0.014 S/cm at 357 K, with an activation energy of 0.64 eV. Garcia-Barriocanal et al. also made a.c. and d.c. conductance measurements on YSZ/STO superlattices and from the collection of data they concluded that the high conductivity measured comes from the interface of the YSZ film with the STO. The activation energies of the interface conductivity of the 30, 5 and 1 nm thin YSZ films in the range, $0.60 \leqslant E_{a,S}^* \leqslant 0.64$ eV, are nearly the same as the independent ion hopping activation energy $E_a \approx 0.52$ eV deduced from bulk conductivity

relaxation data, and $E_{a,QELS} = 0.63$ eV from quasielastic light scattering in bulk YSZ with similar mol% of Y_2O_3. This is unsurprising because of the expected large reduction of ion-ion interaction at the interface and hence also n_S for the interface conduction in nm thin films of YSZ. It follows from (15) that as $n_S \to 0$ on decreasing film thickness down to 1 nm, we have $E_{a,S}^* \to E_a$.

By inspection of Figure 2, it can be seen that $\tau_S^*(T)$ of the nm thin YSZ films are about $2-3$ orders of magnitude shorter than the independent ion hopping relaxation time, τ_0, deduced from bulk ionic conductivity. Garcia-Barriocanal et al. suggested the cause of this enhancement is the large in-plane expansive strain on the YSZ interface plane, which gives rise to higher concentration of vacant oxygen positions and probable positional disorder. Pennycook et al. [58,59] performed simulated annealing to determine the structure of the STO-YSZ multilayers and confirm that the oxygen sublattice near the interface remains highly disordered all the way down to 360 K. From their examination of the energetic of oxygen vacancies at the YSZ interfacial plane, Pennycook et al. concluded that vacancy hopping, and therefore ionic conduction, occurs preferentially in a region adjacent to the interfacial plane, where the O atoms are perturbed but unconstrained by the STO. The importance of structural disorder in determining ionic transport properties in YSZ films with nanoscale thickness has been recently highlighted from a recent atomistic simulation study by Sankaranarayanan and Ramanathan [69]. Because the oxygen sublattice near the interface is highly disordered, an activation entropy enters into determination of the independent hopping frequency, $1/\tau$, which changes (2) to

$$1/\tau_0(T) = (\tau_\infty)^{-1} \exp(-E_a/kT) \exp(\Delta S/k). \quad (18)$$

The activation entropy term, $\exp(\Delta S/k)$, increases the independent hopping frequency of oxygen at the interface of the nm thin film of YSZ, and accounts for the observation that $\tau_S^*(T)$ of the nm thin YSZ films are about $2-3$ orders of magnitude shorter than the independent ion hopping relaxation time, τ_0, deduced from bulk ionic conductivity. Disorder of the oxygen sublattice near the interface caused by lattice-mismatch strain and hence the activation entropy, ΔS, may increase with temperature. If so, this can explain the deviation from Arrhenius temperature dependence of $\tau_S^*(T)$ of the nm thin YSZ films at higher temperatures in Figure 1, and the effective activation energy of the 1 nm YSZ film (0.64 eV) is slightly larger than the actual energy barrier of 0.52 eV deduced from conductivity relaxation in bulk YSZ.

4 Summary and conclusion

The experimental data on dynamics of oxygen ions in bulk YSZ accumulated up to 1998 have already been challenging enough for explanation. The temperature dependences of the d.c. conductivity and the oxygen ion hopping relaxation times from quasielastic light scattering obtained at lower temperatures are Arrhenius. However the prefactors of the Arrhenius T-dependence for both

quantities imply that the oxygen attempt frequency is anomalously high to be accepted to be physically meaningful. The anomaly was attributed to the effect originating from oxygen ion-oxygen ion interaction, which changes the independent oxygen hopping rate. As accounted for by the Coupling Model (CM) in 1998 [25], one consequence is that the attempt frequency is no longer that associated with a vibrational mode and it becomes unphysically high as observed. Another consequence is that the observed activation energy is larger than actual energy barrier opposing the independent hop of oxygen ion. The CM also predicts the crossover from the anomalous properties of the interacting ion-ion dynamics back to independent ion dynamics at high temperatures when the relaxation time becomes shorter than $t_c \approx 1$ to 2 ps. This predicted feature was observed in d.c. conductivity of YSZ (also in other glassy and crystalline ionic conductors, see Ref. [32]) measured at high temperatures where its temperature dependence becomes weaker than the Arrhenius dependence established at lower temperatures. The corresponding conductivity relaxation time $\tau^*(T)$ is approaching and even shorter than t_c, and its prefactor and activation energy are nearly the same as that of the independent ion hop.

The CM explanation of the ion dynamics of bulk YSZ summarized in the above was quantitative in nature, including the prediction of the actual energy barrier, E_a, for independent ion hop was made. The various computer simulations published by different groups in recent years have provided more data on the oxygen ion dynamics in bulk YSZ. The data are in accord with the CM explanation, and in particular have supported the prediction on value of the actual energy barrier E_a. The experimental and computer simulation studies of oxygen ion dynamics in nanometer thin films have shown high conductivity contributed at the surface/interface. It is due to reduction of ion-ion interaction and disordering of the oxygen sublattice near the interface. The increase of conductivity or equivalently the decrease of $\tau^*(T)$ on decreasing film thickness are accounted for in the CM by the decrease of the ion-ion coupling parameter at the surface/interface. The activation energy of surface/interface conductivity in nm thin films, $E_{a,S}^*$, is significantly smaller than E_a^* of conductivity in bulk YSZ with the same mol% Y_2O_3. The fact that $E_{a,S}^*$ becomes comparable to the predicted value of the energy barrier for independent ion hop, E_a, is consistent with the prediction of the CM.

Before closing, it is worthwhile to reiterate that the CM explanation of oxygen ion dynamics in YSZ given here is not an isolated incident. The applications of the CM to similar ion dynamic properties have success in other glassy and crystalline ionic conductors [39,46]. Among these cases is the oxygen ion conductors of pyrochlore structure [28,37–39,51] having compositions, $A_2Zr_{2-y}Ti_yO_7$ (A = Y, Dy, and Gd), which are directly related to YSZ with 33 mol% yttria, $Y_2Zr_2O_7$ $(0.33Y_2O_3-0.67ZrO_2)$. The activation energy barrier predicted by the CM from the conductivity relaxation data was verified by molecular dynamics simulations.

References

1. D. Steele, B.E.F. Fender, J. Phys. C: Solid State Phys. **7**, 1 (1974)

2. C.R.A. Catlow, A.V. Chadwick, G.N. Greaves, L.M. Moroney, J. Am. Ceram. Soc. **69**, 272 (1986)

3. B.W. Veal, A.G. McKale, A.P. Paulikas, S.J. Rothman, L.J. Nowicki, Physica B **150**, 234 (1988)

4. J.E. Bauerle, J. Hrizo, J. Phys. Chem. Solids **30**, 565 (1969)

5. R.E.W. Casselton, Phys. Stat. Sol. **2**, 571 (1970)

6. J.M. Dixon, L.D. La Grange, U. Merten, C.F. Miller, J.T. Porter, J. Electrochem. Soc. **110**, 276 (1963)

7. H. Näfe, Solid State Ion. **13**, 255 (1984)

8. S. Shin, M. Ishigame, Phys. Rev. B **34**, 8875 (1986)

9. J.D. Solier, I. Cachadiña, A. Dominguez-Rodriguez, Phys. Rev. B **48**, 3704 (1993)

10. D.W. Strickler, W.G. Carlson, J. Amer. Ceram. Soc. **47**, 122 (1964)

11. T. Suemoto, M. Ishigame, Phys. Rev. B **33**, 2757 (1986)

12. C. León, M.L. Lucía, J. Santamaría, Phys. Rev. B **55**, 882 (1997)

13. A. Pimenov, J. Ullrich, P. Lunkenheimer, A. Loidl, C.H. Ruscher, Solid State Ion. **109**, 111 (1998)

14. A. Rivera, J. Santamaría, C. León, Appl. Phys. Lett. **78**, 610 (2001)

15. C. León, P. Lunkenheimer, K.L. Ngai, Phys. Rev. B **64**, 184304 (2001)

16. M. Kilo, C. Argirusis, G. Borchardt, R.A. Jackson, Phys. Chem. Chem. Phys. **5**, 2219 (2003)

17. R. Krishnamurthy, Y.G. Yoon, D.J. Srolovitz, R. Car, J. Am. Ceram. Soc. **87**, 1821 (2004)

18. R. Pornprasertsuk, P. Ramanarayanan, C.B. Musgrave, F.B. Prinz, J. Appl. Phys. **98**, 103513 (2005)

19. R. Devanathan, W.J. Weber, S.C. Singhal, J.D. Gale, Solid State Ion. **177**, 1251 (2006)

20. F. Pietrucci, M. Bernasconi, A. Laio, M. Parrinello, Phys. Rev. B **78**, 094301 (2008)

21. A.C.T. van Duin, B.V. Merinov, S.S. Jang, W.A. Goddard III, J. Phys. Chem. A **112**, 3133 (2008)

22. Eunseok Lee, Friedrich B. Prinz, Wei Cai, Phys. Rev. B **83**, 052301 (2011)

23. Kah Chun Lau, Brett I Dunlap, J. Phys.: Condens. Matter **23**, 035401 (2011)

24. A. Tarancón, A. Morata, F. Peiró, G. Dezanneau, Fuel Cells **1**, 26 (2011)

25. K.L. Ngai, Philos. Mag. B **77**, 187 (1998)

26. I. Kosacki, C.M. Rouleau, P.F. Becher, J. Bentley, D.H. Lowndes, Solid State Ion. **176**, 1319 (2005)

27. J. Garcia-Barriocanal, A. Rivera-Calzada, M. Varela, Z. Sefrioui, E. Iborra, C. Leon, S.J. Pennycook, J. Santamaria, Science **321**, 676 (2008)

28. J. Garcia-Barriocanal, A. Rivera-Calzada, M. Varela, Z. Sefrioui, M.R. Diaz-Guilln, K.J. Moreno, J.A. Diaz-Guillen, E. Iborra, A.F. Fuentes, S.J. Pennycook, C. Leon, J. Santamaria, Chem. Phys. Chem. **10**, 1003 (2009)

29. A. Rivera-Calzada, M.R. Diaz-Guillen, O.J. Dura, G. Sanchez-Santolino, T.J. Pennycook, R. Schmidt, F.Y. Bruno, J. Garcia-Barriocanal, Z. Sefrioui, N.M. Nemes, M. Garcia-Hernandez, M. Varela, C. Leon, S.T. Pantelides, S.J. Pennycook, J. Santamaria, Adv. Mater. **23**, 5268 (2011)

30. K.L. Ngai, C. León, Phys. Rev. B **60**, 9396 (1999)

31. K.L. Ngai, C. León, J. Non-Cryst. Solids **315**, 124 (2003)

32. K.L. Ngai, G.N. Greaves, C.T. Moynihan, Phys. Rev. Lett. **80**, 1018 (1998)

33. K.L. Ngai, U. Strom, Phys. Rev. B **38**, 10350 (1988)

34. K.L. Ngai, J. Habasaki, C. León, A. Rivera, Z. Phys. Chem. **219**, 47 (2005)

35. K.L. Ngai, C. León, Phys. Rev. B **66**, 064308 (2002)

36. J. Habasaki, K.L. Ngai, J. Non-Cryst. Solids **352**, 5170 (2006)

37. J.A. Diaz-Guillen, M.R. Diaz-Guillen, J.M. Almanza, A.F. Fuentes, J. Santamaria, C. Leon, J. Phys.: Condens. Matter **19**, 356212 (2007)

38. M.R. Diaz-Guillen, K.J. Moreno, J.A. Diaz-Guillen, A.F. Fuentes, K.L. Ngai, J. Garcia-Barriocanal, J. Santamaria, C. Leon, Phys. Rev. B **78**, 104304 (2008)

39. C. Leon, J. Habasaki, K.L. Ngai, Z. Phys. Chem. **223**, 1311 (2009)

40. *Hamiltonian Dynamic Systems*, edited by R.S. McKay, J.D. Meiss (Adam Hilger, Bristol, 1987)

41. M.C. Gutzwiller, *Chaos in Classical and Quantum Mechanics* (Springer, New York, 1990)

42. K.L. Ngai, Comment Solid State Phys. **9**, 141 (1979)

43. K.Y. Tsang, K.L. Ngai, Phys. Rev. E **54**, R3067 (1996)

44. K.Y. Tsang, K.L. Ngai, Phys. Rev. E **56**, R17 (1997)

45. K.L. Ngai, K.Y. Tsang, Phys. Rev. E **60**, 4511 (1999)

46. K.L. Ngai, *Relaxation and Diffusion in Complex Systems* (Springer, New York, 2011)

47. K.L. Ngai, R.W. Rendell, H. Jain, Phys. Rev. B **30**, 2133 (1984)

48. G. Jarosz, M. Mierzwa, J. Ziozo, M. Paluch, H. Shirota, K.L. Ngai, J. Phys. Chem. B **115**, 12709 (2011)

49. Z. Wojnarowska, C.M. Roland, A. Swiety-Pospiech, K. Grzybowska, M. Paluch, Phys. Rev. Lett. **108**, 015701 (2012)

50. A. Rivera-Calzada, K. Kaminski, C. Leon, M. Paluch, J. Phys. Chem. B **112**, 3110 (2008)

51. K.J. Moreno, G. Mendoza-Suárez, A.F. Fuentes, J. García-Barriocanal, C. León, J. Santamaria, Phys. Rev. B **71**, 132301 (2005)

52. P.J. Wilde, C.R.A. Catlow, Solid State Ion. **112**, 173 (1998)

53. P.J. Wilde, C.R.A. Catlow, Solid State Ion. **112**, 185 (1998)

54. R.E. Williford, W.J. Weber, R. Devanathan, J.D. Gale, J. Electroceram. **3**, 409 (1999)

55. M. Pirzada, R.W. Grimes, L. Minervini, J.F. Maguire, K.E. Sickafus, Solid State Ion. **140**, 201 (2001)

56. F.S. Howell, R.A. Bose, P.B. Macedo, C.T. Moynihan, J. Phys. Chem. **78**, 639 (1974)

57. Kai-Shiun Chang, Yi-Feng Lin, Kuo-Lun Tung, J. Power Source **196**, 9322 (2011)

58. T.J. Pennycook, M.J. Beck, K. Varga, M. Varela, S.J. Pennycook, S.T. Pantelides, Phys. Rev. Lett. **104**, 115901 (2010)

59. T.J. Pennycook, M.P. Oxley, J. Garcia-Barriocanal, F.Y. Bruno, C. Leon, J. Santamaria, S.T. Pantelides, M. Varela, S.J. Pennycook, Eur. Phys. J. Appl. Phys. **54**, 33507 (2011)
60. R.A. De Souza, A. Ramadan, S. Hörner, Energy Environ. Sci. **5**, 5445 (2012)
61. S. Ramanathan, J. Vac. Sci. Technol. A **27**, 1126 (2009)
62. E. Fabbri, D. Pergolesi, E. Traversa, Sci. Technol. Adv. Mater. **11**, 054503 (2010)
63. P. Mondal, A. Klein, W. Jaegermann, H. Hahn, Solid State Ion. **118**, 331 (1999)
64. J. Maier, Solid State Ion. **131**, 13 (2000)
65. N. Sata, K. Eberman, K. Eberl, J. Maier, Nature **408**, 946 (2000)
66. X. Guo, Science **324**, 465.1 (2009)
67. J. Garcia-Barriocanal, A. Rivera-Calzada, M. Varela, Z. Sefrioui, E. Iborra, C. Leon, S.J. Pennycook, J. Santamaria, Science **324**, 465.2 (2009)
68. J.A. Kilner, Nat. Mater. **7**, 838 (2008)
69. S.K.R.S. Sankaranarayanan, S. Ramanathan, J. Chem. Phys. **134**, 064703 (2011)